Mixed Conducting Membranes — Macrostructure Related Oxygen Permeation Flux

Barbara Zydorczak and Kang Li
Dept. of Chemical Engineering and Technology, Imperial College London, South Kensington, London SW7 2AZ, U.K.

Xiaoyao Tan
Dept. of Chemical Engineering and Technology, Imperial College London, South Kensington, London SW7 2AZ, U.K., and School of Environmental and Chemical Engineering, Tianjin Polytechnic University, Tianjin 300160, P.R. China

DOI 10.1002/aic.12216
Published online April 20, 2010 in Wiley Online Library (wileyonlinelibrary.com).

The influence of the macrostructures of LSCF hollow fiber membranes on oxygen permeation flux was investigated experimentally and theoretically. According to the results, asymmetric membranes perform differently toward oxygen permeation depending on their sintering outcome. If both, outer and inner surfaces of the asymmetric membrane are fully densified, finger-like pores become dead volume, which has adverse effects, and the oxygen permeation flux is similar to that of the symmetric membrane. This implies that the improved bulk diffusion due to the reduced membrane thickness is compromised by the additional exchange reaction resistance from the enclosed macrovoids in the asymmetric membranes. However, when one surface of the membrane is fully open, then oxygen permeation is greatly enhanced mainly due to the remarkable increase in the effective surface area for surface exchange reactions. In order to evaluate the actual surface exchange area due to the presence of the porous structure within the asymmetric membranes, a correction factor α, has been introduced in the theoretical analysis presented. © 2010 American Institute of Chemical Engineers *AIChE J,* 56: 3084–3090, 2010

Keywords: mixed conducting membranes, oxygen permeation flux, LSCF hollow fibers, symmetric structure, asymmetric structure, sandwich-like structure

Introduction

Dense mixed conducting membranes prepared from perovskite-type oxides have been studied extensively due to their high-oxygen permeation rates without the need of electrodes. The driving force for oxygen-ion transport is facilitated by the oxygen partial pressure difference across the membrane at elevated temperatures. Since no species other than oxygen can be transferred through the membrane, the oxygen permselectivity is theoretically infinite.[1] This unique characteristic makes the mixed conducting membranes a promising and simple method for oxygen separation from air.

Mixed conducting hollow fiber membranes are usually prepared via well known phase inversion and sintering

Correspondence concerning this article should be addressed to K. Li at Kang.Li@imperial.ac.uk.

© 2010 American Institute of Chemical Engineers

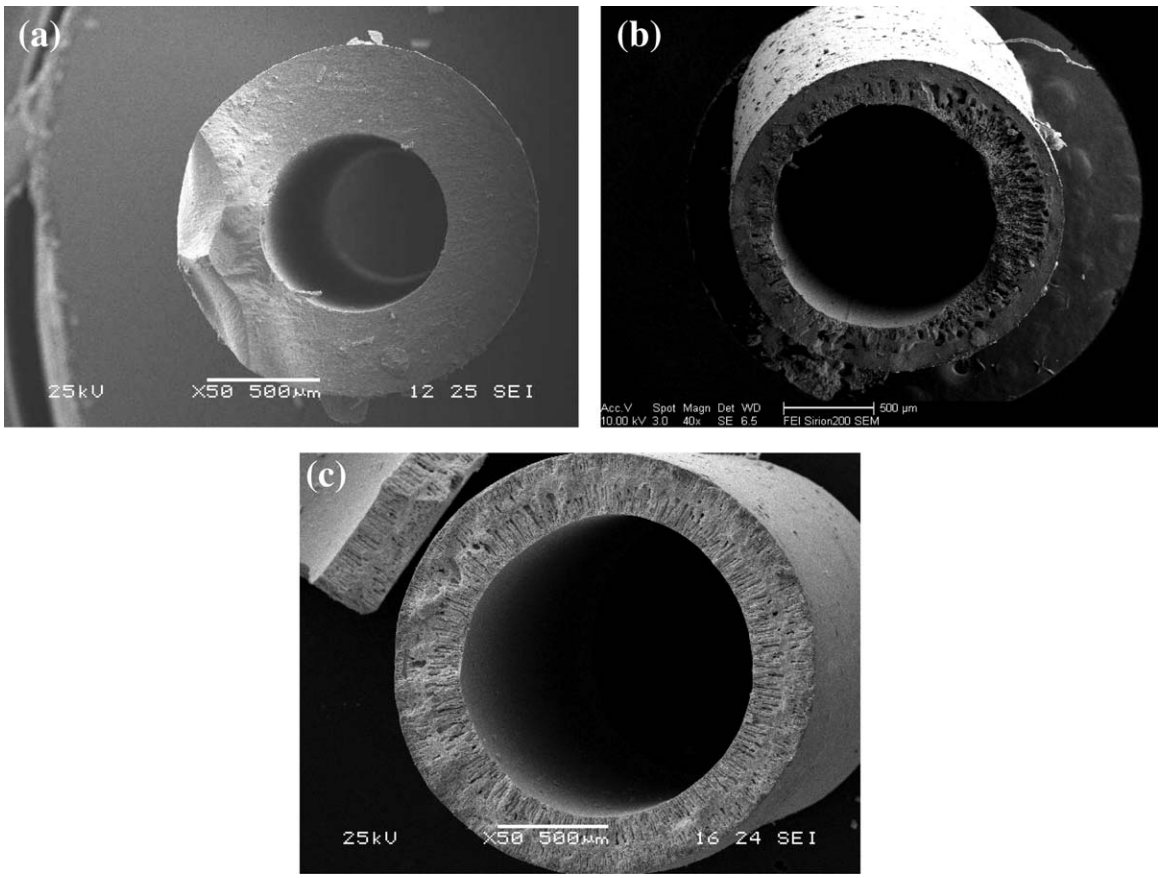

Figure 1. LSCF hollow fiber membranes with different macrostructures.

(a) Symmetric membrane, (b) asymmetric membrane with fingers formed on the inner side of the membrane surface, and (c) asymmetric membrane with fingers formed on both sides of the membrane surface.

technique.[1–6] By changing the preparation conditions, different macrostructures of the membranes can be obtained as shown in Figure 1.Until now, two structures of the LSCF hollow fiber membranes have been prepared (1) symmetric structure that is comprised of a fully dense layer (Figure 1a), and (2) asymmetric structure with fingers (macrovoids) formed on either (Figure 1b) or both sides of the membrane surface (Figure 1c). For example, when water was used as both the internal and external coagulants, a sandwich-like structure, i.e., a central dense layer integrated with fingers on both sides was formed (Figure 1c). However, if the suspension viscosity is increased to a critical value,[7] a symmetric structure without presence of any macrovoids can be obtained as shown in Figure 1a. By properly selecting an internal coagulant media with water being used as the external coagulant, an ultra thin or highly asymmetric structure, which comprised of a dense outside layer supported by fingers fully open toward the inner surface, could be formed as shown in Figure 2.[7] Detailed studies on the formation mechanisms of the aforementioned macrostructures can be found elsewhere.[7,8]

It was found experimentally that the oxygen permeation fluxes through the hollow fibers with different macrostructures varied which indicates that the presence of macrovoids influences greatly the oxygen permeation flux of the fibers. For instance, the macrovoids in the asymmetric hollow fibers are sometimes enclosed in the fiber by the dense surface walls. Consequently, the oxygen permeation through such asymmetric membranes must undergo two additional surface exchange steps while the effective diffusion paths are shortened.

The aim of this study is to evaluate the macrostructure related oxygen permeation. The oxygen permeation through the aforementioned membrane structures were studied both experimentally and theoretically, and the effect of the macrostructure on the oxygen permeation flux was analyzed in detail.

Experimental

Materials

Commercially available $La_{0.6}Sr_{0.4}Co_{0.2}Fe_{0.8}O_{3-\delta}$ (LSCF) powder with the surface area of 6.08 m^2/g and $d_{50} = 0.32$ μm (purchased from Fuel Cell Materials, Lewis Center, OH) was used as the hollow fiber membrane material. Poly(ether sulfone) (PESf, Radel A-300, Solvay Advanced Polymers GmbH, Dusseldorf, Germany) was used as a polymer binder. N-methyl-2-pyrrolidinone (NMP, Synthesis Grade, Merck), and Dimethyl Sulfoxide (DMSO, Sigma Aldrich) were used as solvents in the starting suspensions. Arlacel P135 (Uniquema, Wilton, U.K.) was used as a dispersant. Epoxy

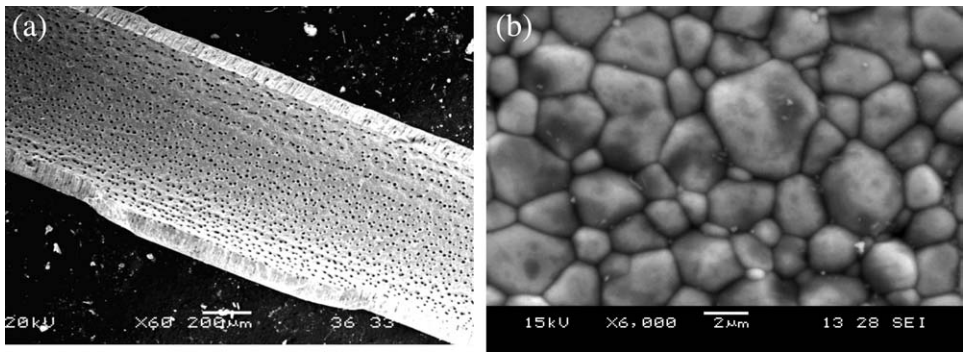

Figure 2. LSCF hollow fiber membranes with an ultrathin structure.

(a) Finger-like pores open toward inner surface, and (b) outer dense surface.

resin sealant (purchased from Fortafix, Ltd., Peterborough, Cambridgeshire, U.K.) was used to assemble the single hollow-fiber membrane.

Oxygen permeation measurement

Different structures of gas-tight LSCF hollow fiber membranes were fabricated using phase inversion/sintering method described elsewhere.[1–7] Before, the oxygen permeation experiments, the LSCF fibers prepared were individually checked for their gas-tightness using an experimental setup described by Tan et al.[1] All the oxygen permeation tests were conducted using a single LSCF hollow fiber membrane. The LSCF hollow fiber membrane was placed on the Al_2O_3 ceramic holder and then placed in a carbolite horizontal tube furnace with the heating zone of 5 cm. The schematic diagram of an apparatus for oxygen permeation measurements is shown elsewhere.[2] Temperature in the furnace was controlled by a microprocessor temperature controller. Glass wool was placed on both ends of the ceramic holder in order to prevent an excessive increase in temperature. Argon was used as a sweep gas fed into the fiber lumen to create the driving force across the hollow fiber membrane. Mass-flow controller was used to control the flow rate of the sweep gas. The oxygen concentration in the effluent was detected by a gas chromatography.

Measurements for the ultrathin membrane were carried out in the temperature range between 1073 K and 1223 K at different sweep gas-flow rates, which were 8.8, 16.8, 24.8, 32.8, 40.8 mL(STP)·min^{-1}, respectively. The maximum oxygen flux of the ultrathin membrane was measured at 1223 K by increasing the sweep gas-flow rate up to 144.9 mL(STP)·min^{-1}. Oxygen permeation measurements for the symmetric and asymmetric membranes (sandwiched and with one porous layer formed close to the inner wall) were conducted in the same temperature range as the ultrathin membrane and at the sweep gas flow rate of 16.8 mL(STP))·min^{-1}. Generally there is a tiny amount of nitrogen present in the effluent because of the leakage of the permeation cell. Assuming nitrogen entered in to the effluent in the form of air, the average oxygen permeation flux over the effective permeation length may be calculated by

$$J_{O_2}^{\exp} = \frac{V_{Ar}}{A_e} \cdot \frac{x_{O_2} - \frac{21}{79} x_{N_2}}{1 - x_{O_2} - x_{N_2}} \tag{1}$$

where V_{Ar} is the volumetric flow rate of Ar gas (mL(STP)·min^{-1}); x_{O2} and x_{N2} are the oxygen and nitrogen concentrations in the effluent determined by GC (V %); A_e is the effective membrane area of the hollow fiber membrane for oxygen permeation $A_e = 2\pi\ (R_o - R_{in})L/\ln\ (R_o/R_{in})$, in which R_o, R_{in}, L are the outer radius, the inner radius and the effective heated length of the hollow fiber membrane, respectively.

Theory

Membrane macrostructure related oxygen permeation

It is well known that the oxygen permeation process through a symmetric mixed conducting membrane from the high oxygen partial pressure side to the low-oxygen partial pressure side includes the following steps in series: (1) mass transfer of gaseous oxygen from the gas stream to the membrane surface (high-pressure side); (2) reaction between the molecular oxygen and oxygen vacancies at the membrane surface (high-pressure side); (3) oxygen vacancy bulk diffusion across the membrane; (4) reaction between lattice oxygen and electron-hole at the membrane surface (low-pressure side), and (5) mass transfer of oxygen from the membrane surface to the gas stream (low-pressure side). The mass-transfer resistances between the gas phase and the membrane surface are generally small compared with the others, and, thus, can be negligible. In addition, the substeps such as oxygen adsorption, dissociation, recombination, and charge transfer can be integrated into the surface exchange kinetics. Consequently, the oxygen permeation flux through the symmetric membrane shown in Figure 3a can be derived as[9]

$$J_{O_2}^{s} = \frac{k_r \left[(p'_{O_2})^{0.5} - (p''_{O_2})^{0.5} \right]}{(p''_{O_2})^{0.5} + \frac{2k_f \delta}{D_V} \cdot (p'_{O_2} p''_{O_2})^{0.5} + (p'_{O_2})^{0.5}} \tag{2}$$

where p'_{O2}, p''_{O2} are the oxygen partial pressures on the upstream and the downstream side, respectively. D_V is the diffusion coefficient of oxygen vacancy; and k_f and k_r are, respectively, the forward and the reverse reaction rate constants for the surface exchange reaction

$$\frac{1}{2} O_2 + V_O^{\cdot\cdot} \overset{k_f/k_r}{\longleftrightarrow} O_O^{x} + 2h^{\cdot} \tag{3}$$

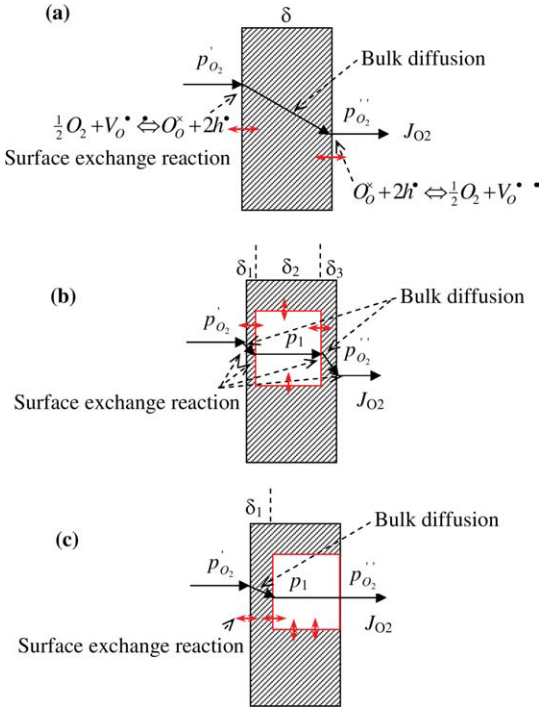

Figure 3. Oxygen permeation process through (a) symmetric structure, (b) asymmetric structure, and (c) highly asymmetric structure.

[Color figure can be viewed in the online issue, which is available at wileyonlinelibrary.com.]

where the charged defects are defined using the Kröger-Vink notation. That is, O_O^x stands for lattice oxygen, $V_O^{\bullet\bullet}$ for oxygen vacancy, and $h_i^{\bullet}$ for electron hole.

In the asymmetric membranes prepared by the phase inversion technique, there are some enclosed macrovoids in the fiber walls. To our knowledge, the exchange reactions take place on the interfaces between the gas oxygen phase and the membrane surface. Accordingly, the oxygen permeation through the asymmetric membrane from the high-oxygen partial pressure side to the low-oxygen partial pressure side undergoes four exchange reaction steps and two bulk diffusion steps in series as shown in Figure 3b. When the exchange reactions on the side surface of the macrovoid are neglected, the overall permeation can be taken as two sequential processes through the two symmetric membranes with the thickness of δ_1 and δ_3, respectively. Consequently, the oxygen flux going across an enclosed macrovoid can be given by the following implicit Eq. 4

$$J_{O_2}^a = \alpha \cdot \frac{k_r\left[(p'_{O_2})^{0.5} - p_1^{0.5}\right]}{(p'_{O_2})^{0.5} + \frac{2k_f\delta_1}{D_V}\cdot(p'_{O_2}p_1)^{0.5} + (p_1)^{0.5}} = \alpha \cdot \frac{k_r\left[p_1^{0.5} - (p''_{O_2})^{0.5}\right]}{(p''_{O_2})^{0.5} + \frac{2k_f\delta_3}{D_V}\cdot(p''_{O_2}p_1)^{0.5} + (p_1)^{0.5}} \quad (4)$$

where α is the correction coefficient to modify the actual surface exchange area due to the presence of the porous structure, and p_1 is the pressure in the enclosed macrovoid.

Obviously, the total oxygen permeation flux through the asymmetric membranes can be given as

$$J_{O_2} = (1-\varepsilon)J_{O_2}^s + \varepsilon J_{O_2}^a \quad (5)$$

where ε is the porosity of the hollow fiber membrane.

For the ultrathin or highly asymmetric membrane, the finger-like pores are open directly to the hollow fiber membrane surfaces. Figure 3c depicts the oxygen permeation process through the ultrathin membranes. As can be seen, the actual membrane thickness for oxygen permeation across the finger-like pore has been reduced to δ_1. Furthermore, since the surface exchange reactions take place on the side interfaces of the finger-like pores, the real membrane area for surface exchange reactions has also been increased remarkably. Considering the change of the membrane surface area for exchange reactions, the oxygen permeation flux through the highly asymmetric membrane can be written as

$$J_{O_2}^h = \alpha \cdot \frac{k_r\left[(p'_{O_2})^{0.5} - (p''_{O_2})^{0.5}\right]}{(p''_{O_2})^{0.5} + \frac{2k_f\delta}{D_V}\cdot(p'_{O_2}p''_{O_2})^{0.5} + (p'_{O_2})^{0.5}} \quad (6)$$

where δ is the effective membrane thickness for oxygen permeation.

Governing equations of the permeation cell

Oxygen permeation through the hollow fiber membrane was conducted by introducing argon as sweep gas in the lumen side, while the membrane outer surface was exposed to the atmosphere. At an elevated temperature, oxygen permeates from the air-side to the sweep gas-side under the oxygen concentration gradient across the membrane. The following assumptions are adopted for the derivation of governing equations of the permeation cell: (1) isothermal operation; (2) plug flow for the lumen stream; (3) independence of the surface exchange rate constants and vacancy diffusion coefficient on oxygen partial pressure, and (4) oxygen partial pressure on the outside of the hollow fiber is constant (21 kPa); 5) ideal gas behavior. The mass conservation equations for the lumen phase can be written as

$$\frac{d}{dl}\left(\frac{p''_{O_2}V}{RT}\right) = 2\pi R_m \cdot J_{O_2}, \text{ for oxygen} \quad (7)$$

$$\frac{(p_t - p''_{O_2})V}{RT} = F_{Ar}, \text{ for argon} \quad (8)$$

with the boundary condition

$$l = 0, \quad p''_{O_2} = 0 \quad (9)$$

where V is the volumetric flow rate of the lumen gas stream, p_t is the pressure in the lumen, $p_t = pa = 1.013 \times 10^5$ Pa, R_m is the logarithmic radius, $R_m = (R_o - R_{in})/\ln(R_o/R_{in})$, F_{Ar} is the molar feed flow rate of sweep gas, R is ideal gas constant, and T is the operating temperature, respectively.

Integration of the governing Eqs. 7–9 gives the oxygen concentration in the outlet of the fiber, with which the average oxygen permeation flux over the effective membrane length can be subsequently obtained.

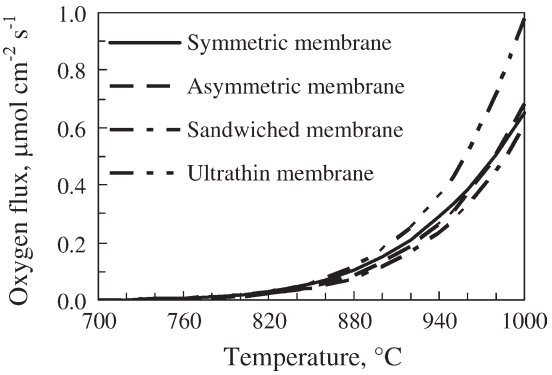

Figure 4. Oxygen permeation flux as a function of temperature under the oxygen partial pressure gradient of 21kPa/2kPa through (a) symmetric membrane (δ = 270 μm), (b) asymmetric membrane (δ_1= 10 μm, δ_2 = 250 μm, δ_3 = 10 μm, ε = 0.5); (c) sandwiched membrane (δ_1 = 10 μm, δ_2 = 120 μm, δ_3 = 10 μm, δ_4 = 120 μm, δ_5 = 10 μm, ε1 = 0.3 and ε2 = 0.3), and (d) highly asymmetric membrane (δ_1 = 10 μm, δ_2 = 260 μm, ε = 0.5).

Results and Discussion

In the beginning, theoretical analysis was performed using the kinetic parameters obtained in the literature.[9] Figure 4 shows oxygen permeation fluxes of the LSCF hollow fiber membranes having the same wall thickness (270 μm in total), but with different macrostructures under the oxygen partial pressure gradient of 21kPa/2kPa. As can be seen, the asymmetric hollow fiber membranes exhibit lower fluxes than the symmetric membrane, but the highly asymmetric membrane possesses the highest fluxes in the whole temperature range. This suggests that the enclosed macrovoids within the membrane wall have yielded negative effects on oxygen permeation especially at lower-temperatures. As mentioned previously, the oxygen permeation through a mixed conducting membrane undergoes three sequential steps, i.e., upstream surface exchange reaction, bulk diffusion and downstream surface exchange reaction. When the oxygen is permeated across a macrovoid structure, the bulk-diffusion resistance is reduced due to the decrease of the effective diffusion route, but two additional surface exchange resistances are produced at the same time. Therefore, whether the overall resistance to oxygen permeation is increased or decreased depends on the relative changes of these two types of resistances. For example, at a lower-temperature, the decrease of the diffusion resistance in asymmetric membranes is much lower than the increase of the exchange reaction resistance, leading to reduced oxygen fluxes. When the temperature is increased to above 1153 K, the decrease of the diffusion resistance will be larger than the increase of the exchange reaction resistance. As a result, the oxygen flux of the asymmetric membrane with single porous structure will be higher than that of the symmetric membrane at the temperatures higher than 1153 K. However, for the highly asymmetric membrane with open finger-like pores, the effective membrane thickness for oxygen transport is noticeably decreased resulting in the improvement of oxygen flux. Such an increase in oxygen flux becomes noticeable at higher-temperatures, because the permeation is controlled by the surface exchange kinetics at lower-temperatures, but the resistance from bulk diffusion plays a more and more important role in oxygen permeation as the temperature is increased.

Figure 5 shows the experimental oxygen fluxes of the symmetric and the sandwiched asymmetric LSCF hollow fiber membranes at temperatures 1073–1223 K, and sweep gas-flow rate of 12.49 μmol s^{-1} (16.8 mL(STP) min^{-1}). It can be seen that the asymmetric membrane exhibited similar oxygen fluxes to the symmetric membranes. This implies that the additional exchange reaction resistance from the enclosed macrovoids in the asymmetric membranes may be equivalent to the decrease of the diffusion resistance due to the reduced membrane thickness. In addition, the theoretical permeation fluxes calculated using the structural parameters of the fibers were also plotted with the lines in Figure 5. As can be seen, the modeling results match the experimental data very well for the symmetric hollow fiber membrane. However, the experimental permeation fluxes of the asymmetric membrane were higher than the theoretical results (α = 1). This is because the exchange reactions also took place on the side interfaces of the enclosed macrovoids, hence, the actual membrane area for exchange reactions might be larger than the hollow fiber's apparent surface area, just as considered in the derivation of Eq. 4. By regressing the experimental fluxes with the mathematical model, the correction coefficient to modify the actual surface exchange area was obtained to be about α = 1.5, with which the modeling results agree very well with the experimental data as shown in Figure 5.

The experimental and the modeling oxygen permeation fluxes of the highly asymmetric or the ultrathin hollow fiber membrane were plotted against temperature in Figure 6. Again, it can be seen that the experimental permeation fluxes are much higher than the theoretical data obtained using the hollow fiber's apparent surface area (α = 1). One reason is that the effective membrane thickness for oxygen transport is noticeably decreased (from 150 μm to around 12 μm) in the highly asymmetric hollow fibers. However, only such decrease in membrane thickness is not enough to yield so large an increase in the permeation flux. For example, the theoretical fluxes with respect to negligible bulk diffusion

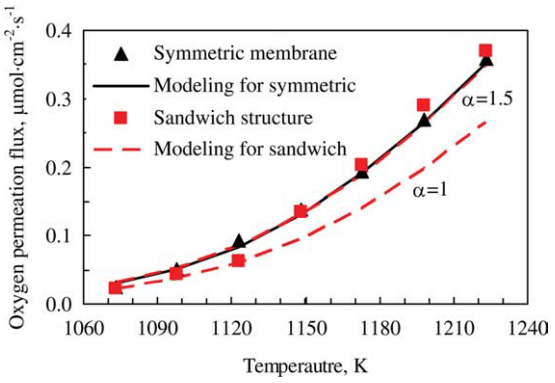

Figure 5. Oxygen permeation rates of the symmetric and the sandwiched hollow fiber membranes as a function of temperature (sweep gas-flow rate = 16.8 mL(STP) min^{-1}).

[Color figure can be viewed in the online issue, which is available at wileyonlinelibrary.com.]

resistance ($\delta = 0$) are still much lower than the experimental data, as shown in Figure 6 with the dashed line. This indicates that the improvement of the oxygen flux in the highly asymmetric membrane is primarily resulted from the increase of the effective surface exchange areas, which promotes the exchange kinetics. However, due to the fact that the macrovoids are fairly irregular in configuration, it is difficult to estimate the real exchange area for reactions. By fitting the experimental data with modeling results, the correction coefficient to modify the actual surface exchange area was estimated to be around 4.93 for the highly asymmetric hollow fiber membranes in this work. Therefore, the ultrathin hollow fiber membranes could provide much larger surface exchange areas than the asymmetric membranes with enclosed macrovoids.

Figure 7 shows the oxygen permeation flux as a function of sweep gas-flow rate at different temperatures for the highly asymmetric hollow fiber membrane. As is expected, the oxygen flux increased with sweep gas rate at a given temperature since a higher sweep rate could increase the driving force for oxygen permeation by lowering the oxygen partial pressure on the permeate side. Using the correction coefficient of surface exchange area obtained before $\alpha = 4.93$, the theoretical permeation fluxes at various experimental conditions were obtained and were also plotted with the lines in Figure 7. As can be seen, the experimental data generally are in good agreement with the theoretical results. However, at lower-temperatures (i.e., 1073 K) or low sweep gas-flow rates (i.e., 6.54 μmol s^{-1} or 8.79 mL(STP) min^{-1}), the deviation of the experimental data from the prediction results is relatively large because the systematic error could be larger under these conditions.

Conclusions

$La_{0.6}Sr_{0.4}Co_{0.2}Fe_{0.8}O_{3-\delta}$ (LSCF) hollow fiber membranes with different macrostructures can be fabricated by changing the composition of the spinning suspension and using different preparation conditions. The macrostructure greatly influences the permeation flux of the hollow fiber membranes by either reducing the effective membrane thickness or increasing the effective exchange reaction areas. At lower-temperatures the enclosed macrovoids within the fiber wall yield large exchange reaction resistance, and, thus, suppress oxygen permeation. However, at higher-temperatures, the additional exchange reaction resistance can be offset by decrease of the bulk diffusion resistance from the reduced membrane thickness. The highly asymmetric membrane exhibited much higher fluxes mainly because of the remarkable increase in the effective area for surface exchange reactions.

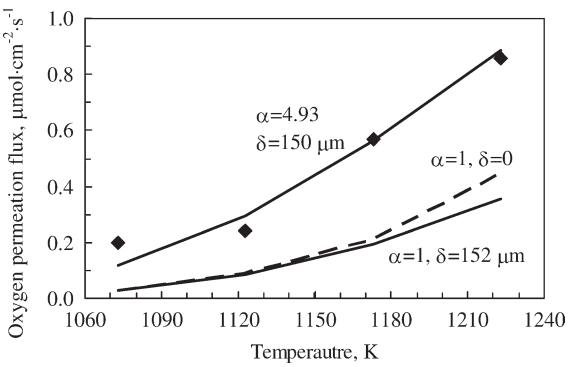

Figure 6. Oxygen permeation flux of the highly asymmetric hollow fiber membranes as a function of temperature (sweep gas-flow rate = 16.8 mL(STP) min^{-1}).

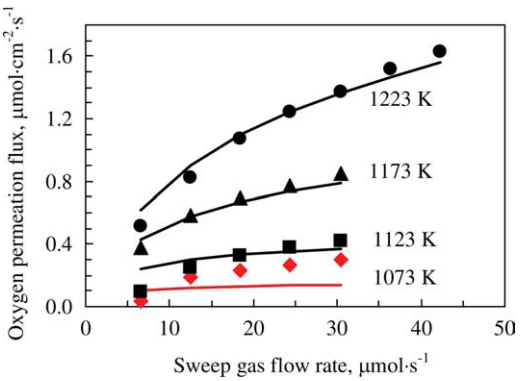

Figure 7. Oxygen permeation rates of the highly asymmetric hollow fiber membranes as a function of sweep gas flow rate at different temperatures (α = 4.93 for calculations).

[Color figure can be viewed in the online issue, which is available at wileyonlinelibrary.com.]

Acknowledgments

The authors gratefully acknowledge the research funding provided by EPSRC in the United Kingdom (EP/E032079/1), and by the National Natural Science Foundation of China (No. 20676073).

Notation

A_e = effective membrane area for oxygen permeation, cm^2
D_V = effective diffusivity of oxygen vacancy, cm^2/s
F = gas-feed flow rate, mol/s
J_{O_2} = oxygen permeation flux, mol/(cm^2 s)
k_r = reverse surface exchange reaction rate constant, mol/(cm^2 s)
k_f = forward surface exchange reaction rate constant, cm/($Pa^{0.5}$ s)
L = effective length of hollow fiber for oxygen permeation, cm
p_1 = pressure in the enclosed macrovoid, Pa
p_a = atmospheric pressure, 1.013×10^5 Pa
p'_{O2}, p''_{O2} = oxygen partial pressure in the air- and the sweep-side, Pa
p_t = pressure in the lumen side, Pa
R = ideal gas constant
R_m = algorithmic radius of fiber
$R_m = (R_o - R_{in})/\ln(R_o/R_{in})$
R_{in}, R_o = inner and outer radius of hollow fiber, cm
T = operating temperature, K
x_{o2}, x_{N2} = oxygen and nitrogen concentrations in sweep side, %
V = volumetric flow rate of the shell and the lumen gas stream, cm^3/s
α = correction coefficient to modify the actual surface exchange area
δ = effective membrane thickness for oxygen permeation
ε = porosity of the hollow fiber membrane

Literature Cited

1. Tan X, Liu Y, Li K. Mixed conducting ceramic hollow fiber membranes for air separation. *AIChE J*. 2005;51:1999–2000.

2. Tan X, Liu Y, Li K. Preparation of LSCF ceramic hollow fiber membranes for oxygen production by a phase inversion/sintering technique. *Ind Eng Chem Res*. 2005;44:61–66.
3. Li K, Tan X, Liu Y. Single-step fabrication of ceramic hollow fibers for oxygen permeation. *J Membr Sci*. 2006;272:1–5.
4. Tan X, Li K. Oxygen production using dense ceramic hollow fiber membrane modules with different operating modes. *AIChE J*. 2007;53:838–845.
5. Tan X, Wang Z, Liu H, Liu S. Enhancement of oxygen permeation through $La_{0.6}Sr_{0.4}Co_{0.2}Fe_{0.8}O_{3-\delta}$ hollow fiber membranes by surface modifications. *J Membr Sci*. 2008;324:128–135.
6. Wang Z, Yang N, Meng B, Tan X. Preparation and oxygen permeation properties of highly asymmetric $La_{0.6}Sr_{0.4}Co_{0.2}Fe_{0.8}O_{3-\alpha}$ perovskite hollow fiber membranes. *Ind Eng Chem Res*. 2009;48:510–516.
7. Zydorczak B, Wu Z, Li K. Fabrication of ultrathin LSCF hollow fiber membranes for oxygen permeation. *Chem Eng Sci*. 2009;64:4383–4388.
8. Kingsbury BFK, Li K. Morphological study of ceramic hollow fiber membranes. *J Membr Sci*. 2009;328:134–140.
9. Xu SJ, Thomson WJ. Oxygen permeation rates through ion-conducting perovskite membranes. *Chem Eng Sci*. 1999;54:3839–3850.

Manuscript received Oct. 15, 2009, and revision received Jan. 22, 2010.